Measurement of Modulational Instability Gain of Second-Order Nonlinear Optical Eigenmodes in a One-Dimensional System

R. Schiek, H. Fang, R. Malendevich, and G. I. Stegeman

School of Optics and Center for Research and Education in Optics and Lasers, University of Central Florida, 4000 Central Florida Boulevard, Orlando, Florida 32816-2700

(Received 10 October 2000)

We have investigated the amplification of a spatially periodic perturbation applied to a wide fundamental beam launched near phase matching for second-harmonic generation in a lithium niobate film waveguide. We measured the gain coefficient for the modulational instability of quadratic eigenmodes as a function of periodicity, intensity, and wave-vector mismatch. Excellent agreement with theory was obtained.

DOI: 10.1103/PhysRevLett.86.4528 PACS numbers: 42.65.Sf, 42.65.Tg

When the response of a medium to wave motion is nonlinear, stationary solutions to the corresponding nonlinear wave equation are the nonlinear eigenmodes with specific relations between their intensity, their propagation constant, and the properties of the medium. If perturbations occur in any of these parameters, certain eigenmodes become unstable leading to breakup of the wave, known as modulational instability (MI) [1]. Temporal and spatial perturbations of unstable eigenmodes with infinite extent in time (cw eigenmodes) or space (plane wave eigenmodes) lead to temporal and spatial MI, respectively, usually triggered by noise on the wave input into the medium. The Fourier components of the noise over a limited and well-defined range of temporal or spatial frequencies grow exponentially with time or propagation distance. The corresponding gain coefficient varies with the frequency and local intensity, and the frequency with the maximum gain coefficient ultimately determines the periodicity of the wave breakup, leading to periodic structures on the output wave.

MI has been observed in many nonlinear systems, for example, in waves in plasmas, electrical circuits, mechanics, fluids, and optics [2,3]. In the optical domain, MI has proven very important because the instability experienced by optical beams and pulses in nonlinear media places an upper limit on the intensity of waves that can propagate unchanged and be used effectively in nonlinear interactions. In fact, one of the first optical nonlinear effects observed was spatial MI, the breakup of broad, high intensity beams into filaments in Kerr media due to spatial noise present on the beam [4]. During the past few decades, a number of experiments with optical waves have been reported in Kerr, photorefractive, and quadratic bulk media in which noise generated spatial MI patterns have been observed [5–7]. The theoretical understanding of MI is well developed. Expressions have been derived for the gain coefficient-periodicity-intensity relation in waveguides [one-dimensional (1D) case] in media with Kerr, photorefractive, and quadratic nonlinearities [8–10]. The analysis is more complex in bulk media in the 2D case where exact analytical expressions are not available [11]. Until this year, the only optical examples of MI in a 1D geometry had been in the temporal domain in optical fibers [3]; until recently 1D MI due to quadratic nonlinearities has been observed also in space domain in slab waveguides [12]. MI patterns generated from seeded perturbations have been predicted, observed in the temporal domain, and shown to develop after further propagation into a train of temporal solitons which are the stable eigenmodes of the system [13–15].

Although the beam breakup due to noise has been observed frequently, there are only a few measurements of the gain coefficients themselves for direct comparison with theory. This requires a controlled seeding of the beam with a periodic modulation and measurement of the growth of the seed before saturation and soliton formation sets in. For example, temporal modulation of surface plasma waves has been investigated but the interpretation was hampered by the multiplicity of nonlinear mechanisms present [16]. To the best of our knowledge, the relation between periodicity, gain, and intensity has not been explored experimentally and compared successfully with theory, even for the simplest 1D case where analytical theories exist. We have chosen to investigate the gain coefficients of spatial MI in a 1D medium with a quadratic nonlinearity. This is an especially rich system because, near the condition for phase-matched second-harmonic generation (SHG), the eigenmodes consist of coupled fundamental (FD) and second-harmonic (SH) waves and, hence, the gain coefficient depends on yet another variable, the phase mismatch $\Delta\beta L$. $\Delta\beta = 2\beta_{\mathrm{FD}} - \beta_{\mathrm{SH}}$ is the wave-vector mismatch, and L is the sample length. In this work, we seeded a periodic perturbation on a broad beam injected into a lithium niobate ($LiNbO_3$) slab waveguide near its phase-matching condition for SHG. The growth of the perturbation was measured at the waveguide output, yielding what we believe to be the first quantitative measurement of the MI growth rate or gain coefficient for comparison with theory.

 0031-9007/01/86(20)/4528(4)$15.00

The MI analysis in 1D is based on the periodic perturbation of the appropriate "plane wave" nonlinear eigenmodes of a film waveguide. For quadratically nonlinear media, they consist of both a FD and SH wave, both extended infinitely wide in the transverse direction parallel to the film. The fields are locked in phase ("P-branch" eigenmode) or out of phase ("N-branch") with one another so that there is no net energy exchange between FD and SH [17]. Trillo and co-workers have shown that eigenmodes of both branches in a slab waveguide (1D geometry) are not stable solutions of the nonlinear coupled wave equations describing SHG [10]. A small sinusoidal perturbation of the eigenmode with a periodicity Λ in the transverse direction on a wide input beam grows exponentially with a gain γ for specific spatial frequencies $2\pi/\Lambda$ as long as the perturbation amplitude is small compared to the eigenmode amplitude itself. Substitution of the perturbed eigenmode into the coupled wave equations under the assumption that the eigenmode amplitude is much larger than the perturbation amplitude yields a linear system of equations for the initial evolution of the periodic perturbation of the beam. For a positive eigenvalue γ, the perturbation grows. The corresponding eigenvector has similar real and imaginary parts, so that amplitude as well as phase noise or seeded perturbations will be amplified. Also, it does not matter if the noise is in the FD, SH, or in both. The theory provides predictions for the relationship between the gain coefficient, the intensity, the periodicity, and the phase mismatch [10]. Figure 1 shows the theoretically predicted dependence of the gain on the periodicity for typical experimental parameters.

The experiments were performed with a double-pass LBO-based OPG/OPA system pumped by a frequency-doubled, Q-switched, active/passive mode-locked Nd:YAG laser at 532 nm. It provided 20-ps-long pulses at a FD wavelength of 1.32 μm with a repetition rate 10 Hz. A 650×8 μm^2 wide elliptical beam (full width at half maximum) was coupled into the $L = 47$ mm long, Y-cut X-propagating, titanium-indiffused lithium niobate slab waveguide. The FD was a TM_0 waveguide mode and the SH a TE_1 mode. To satisfy type-I phase matching, the waveguide was heated in an oven to around 340 °C. Because of temperature and waveguide parameter variations along the crystal, the wave-vector mismatch increases towards the waveguide ends. We investigated MI of the long-wave-type of only the N-branch eigenmodes in the positive wave-vector mismatch range, because they were the only nonlinear eigenmodes that could be easily excited without SH seeding in our wave-vector mismatch profile. The amount of SH required for this eigenmode was adiabatically generated in the nonuniform wave-vector mismatch profile region near the input [18] over a distance short compared to any significant growth of the amplitude modulation. This effectively immediate generation of the eigenmode was verified by numerical modeling of the coupled wave system for our input and experimental conditions.

In order to measure the gain, the input FD beam was seeded with a periodic perturbation with a well-defined amplitude and periodicity. The experimental setup is shown in Fig. 2. The seeding beam (path with mirror M and filter F) represents a periodic phase perturbation for the main beam. Mirror M and filter F were used to adjust periodicity and power of the perturbation. The two input beams with equal width were aligned carefully to overlap in time and space, and produce well-defined interference fringes. For a 650 μm wide beam, a maximum intensity (power per waveguide width) of 180 W/μm in the beam center could be launched which corresponds to a peak power of 125 kW in the whole beam and 2.7 μJ energy in the 20-ps-long pulse. Cylindrical lens combinations were used to form the elliptical input beam. The beam profiles at the waveguide's input and output facets were measured with a camera for both different input powers and different positive wave-vector mismatches.

Figure 3 shows corresponding numerical simulations of cw beam propagation along the waveguide for a 100 μm perturbation period and a power ratio between the beams of 100:0.16. For all simulations, the details of the experiment such as losses, nonuniform wave-vector mismatch, input beam noise, lack of SH seeding, finite beam width, and film characteristics, except only the pulsed input, were taken into account. Although the existence of $\chi^{(3)}$, in general, modifies the eigenmodes and MI [10], its typical values in $LiNbO_3$ are small and can be neglected for our

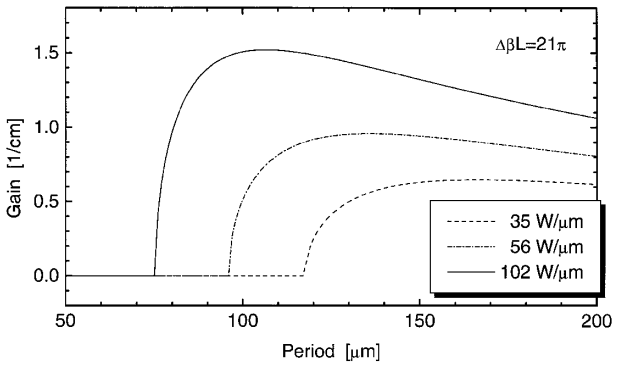

FIG. 1. Gain for N-branch modes versus periodicity for different eigenmode FD intensities.

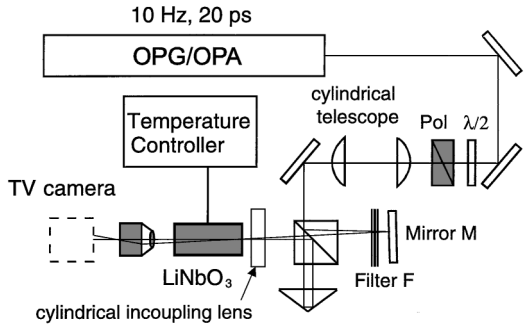

FIG. 2. Experimental setup for seeding the main input beam with a small periodic perturbation.

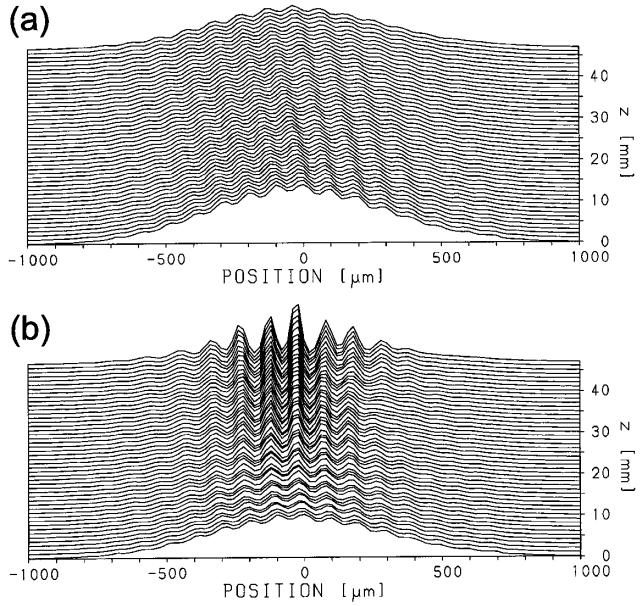

FIG. 3. Numerical simulation of low power (a) and high power (b) beam propagation for a phase mismatch of $\Delta\beta L = 21\pi$ at a temperature of 334 °C for two interfering beams with a power ratio of 100:0.16. The peak input intensity in (b) is 63 W/μm.

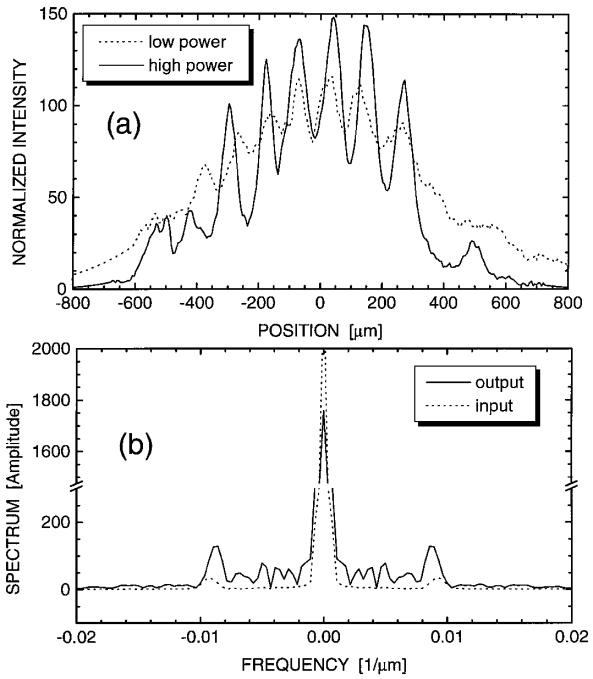

FIG. 4. (a) Normalized low power (6 W/μm) and high power (120 W/μm) output beams, both with a 110 μm periodic perturbation at the input. (b) Spatial spectra of the square root of the intensity of the high power (120 W/μm) input and output beams that show the magnification of the perturbation spectral components at the spatial frequency $\pm 0.009\ \mu\text{m}^{-1}$. The phase mismatch is 21π at 334 °C.

experimental conditions. Figure 3(a) shows an example of low power beam propagation. Because of the beam crossing geometry, the seeding beam walks out of the main beam towards the left side with its center shifted at the output to a position of -280 μm. Interference fringes are obtained all along the propagation as long as the two beams overlap. MI sets in with increasing power and the linear interference pattern does no longer dominate the pattern characteristics. In Fig. 3(b), the result of a simulation with a peak intensity of 63 W/μm is shown. After a few mm of propagation, the perturbation grows due to the MI gain above the level of the initial linear interference fringes. It is a characteristic of the MI that the lines of intensity maxima of the pattern are no longer tilted relative to the main beam direction. Now, the amplified perturbation, with maxima locked at the positions where they were seeded, dominate the picture.

Although it is not possible to observe the beam propagation along the waveguide since it is housed in an oven, MI was detected by comparing the input and output beam profiles. At low powers, the input and output intensity distributions including perturbation amplitudes and periods are very similar. Typical output beams for a low and a high power input with a perturbation periodicity of 110 μm and a phase mismatch of $\Delta\beta L = 21\pi$ (at a crystal temperature of 334 °C) are shown in Fig. 4(a). It is clear that the seeded input perturbation is amplified at high power. Because of the temporal averaging over the pulses, the contrast ratio of the fringes is reduced compared to the cw simulation. Note that the high power fringes in the beam wings show the power-dependent shift relative to the low power ones, as predicted in the simulations. Although this is difficult to recognize in the experiments with the 110 μm periodicity because there the fringe-position shift equals the periodicity, the position-locking phenomenon was easily verified in experiments with 175 μm periodicity. We verified that the output beam modulation was initiated by the seeded perturbation and not by random noise induced MI by blocking the weak perturbation beam. We proved that the modulation disappears when the perturbation seed is switched off.

In order to quantify the MI gain, the field scans were Fourier transformed. Typical input and output spatial Fourier spectra are compared in Fig. 4(b). The side lines at $\pm 0.009\ \mu\text{m}^{-1}$ in the Fourier spectrum represent the perturbation and are a measure of the amplification of the perturbation. The gain coefficient can be estimated from the peaks at the perturbation frequency using the following equation:

$$\gamma(f) = L^{-1} \ln[S_{\text{out}}(f)/S_{\text{in}}(f)]. \qquad (1)$$

L is the waveguide length, S is the spectral amplitude, and f is the spatial perturbation frequency. The gain measurements were performed only at power levels where the MI pattern does not saturate and the net growth of the sinusoidal pattern is small.

The gain measurement results are shown in Figs. 5 and 6. In Fig. 5, power-dependent gain coefficients for different perturbation periods for a constant phase mismatch of 21π (at 334 °C) are compared. For a perturbation periodicity below 85μm, we could not amplify

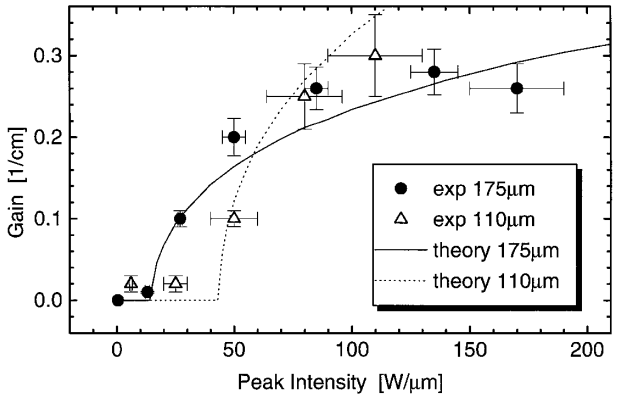

FIG. 5. Dependence of the MI gain coefficient on input peak intensity for two different perturbation periods at a constant phase mismatch of 21π at 334 °C. Experimental data are in scattered points: (●) 175 μm; (Δ) 110 μm. Theoretical simulations are the solid (175 μm) and dotted (110 μm) curves.

any seeded perturbation, which is in agreement with the theory which predicts a threshold periodicity of 75 μm below which the MI gain is zero for this wave-vector mismatch and our intensity levels (see Fig. 1). Figure 6 shows the dependence of the gain on the wave-vector mismatch for fixed periodicity. As expected, the MI gain decreases for increasing wave-vector mismatch together with the nonlinear phase shifts produced by the cascaded nonlinearity which are responsible for the instability of the second-order nonlinear eigenmodes. Numerical simulations that included nonideal experimental conditions were used to show empirically that the measured gain coefficient is reduced by a factor of about 5 from its ideal value due to finite beam width, nonuniform wave-vector mismatch, waveguide losses, lack of SH seeding, and pulsed instead of cw input. This factor is included in the theoretically calculated gain curves in Figs. 5 and 6 to compare to our experiment (compare Fig. 1 to Figs. 5 and 6). Note that, for a detuning of 145π, the SH component

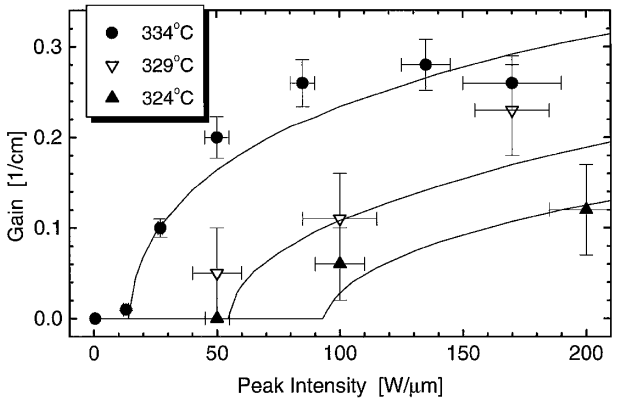

FIG. 6. Dependence of the MI gain coefficient on input peak intensity for three different phase mismatches and a constant perturbation periodicity of 175 μm. Experimental data are in scattered points: (●) $\Delta\beta L = 21\pi$ at 334 °C; (∇) 83.7π at 329 °C; (▲) 145.5π at 324 °C. Simulation results are shown with solid curves.

is very small and the results mimic closely that for a Kerr nonlinearity.

In conclusion, we have investigated seed-induced MI of second-order nonlinear eigenmodes in $LiNbO_3$ slab waveguides. By comparing the spectra of the output and input fields, the power- and periodicity-dependent gain coefficient was measured for different wave-vector mismatch conditions. The results are in good quantitative agreement with theory.

The research was supported by NSF and an ARO MURI.

[1] See, for example, E. Enfield and G. Rowlands, *Nonlinear Waves, Solitons and Chaos* (Cambridge University, Cambridge, England, 1990).
[2] T. Taniuti and H. Washimi, Phys. Rev. Lett. **21**, 209 (1968); J. M. Bilbaut, P. Marquie, and B. Michaux, Phys. Rev. E **51**, 817 (1995); A. H. Nayfeh and D. T. Mook, *Nonlinear Oscillations* (Wiley, New York, 1979); G. B. Whitman, J. Fluid Mech. **22**, 273 (1965).
[3] K. Tai, H. Hasegawa, and A. Tomita, Phys. Rev. Lett. **56**, 135 (1986).
[4] For an early review, see S. A. Akhmanov, R. V. Khokhlov, and A. P. Sukhorukov, *Laser Handbook,* edited by F. T. Arecchi and E. O. Schulz-DuBois (North-Holland, Amsterdam, 1972), pp. 1151–1228.
[5] A. J. Campillo, S. L. Shapiro, and B. R. Suydam, Appl. Phys. Lett. **23**, 628 (1973).
[6] A. V. Mamaev, M. Saffman, and A. A. Zozulya, Phys. Rev. Lett. **76**, 2262 (1996); D. Kip, M. Soljajic, M. Segev, E. Eugenieva, and D. N. Christodoulides, Science **290**, 495 (2000).
[7] R. A. Fuerst, D.-M. Baboiu, B. Lawrence, W. E. Torruellas, G. I. Stegeman, S. Trillo, and S. Wabnitz, Phys. Rev. Lett. **78**, 2756 (1997).
[8] A. Hasegawa and W. F. Brinkman, IEEE J. Quantum Electron. **16**, 694 (1980).
[9] A. V. Mamaev, M. Saffman, D. Z. Anderson, and A. A. Zozulya, Phys. Rev. A **54**, 870 (1996); M. Soljacic, M. Segev, T. Coskun, D. N. Christodoulides, and A. Viswanath, Phys. Rev. Lett. **84**, 467 (2000).
[10] S. Trillo and P. Ferro, Opt. Lett. **20**, 438 (1995); Phys. Rev. E **51**, 4994 (1995); S. Trillo and S. Wabnitz, Phys. Rev. E **55**, R4897 (1997); S. Trillo, A. V. Buryak, and Y. S. Kivshar, Opt. Commun. **122**, 200 (1996).
[11] D.-M. Baboiu and G. I. Stegeman, Opt. Quantum Electron. **30**, 937 (1998).
[12] H. Fang, R. Malendevich, R. Schiek, and G. I. Stegeman, Opt. Lett. **25**, 1786 (2000).
[13] A. Hasegawa, Opt. Lett. **9**, 288 (1984).
[14] K. Tai, A. Tomita, J. L. Jewell, and A. Hasegawa, Appl. Phys. Lett. **49**, 236 (1986).
[15] P. V. Mamyshev, S. V. Chernikov, E. M. Dianov, and A. M. Prokhorov, Opt. Lett. **15**, 1365 (1990).
[16] D. Grozev, A. Shivarova, and S. Taney, J. Plasma Phys. **45**, 297 (1991); D. Grozev, K. Kirov, K. Makasheva, and A. Shivarova, IEEE Trans. Plasma Sci. **25**, 415 (1997).
[17] A. E. Kaplan, Opt. Lett. **18**, 1223 (1993).
[18] R. Schiek, Y. Baek, and G. I. Stegeman, J. Opt. Soc. Am. B **15**, 2255 (1998).